ACS Catalysis

RESEARCH ARTICLE

pubs.acs.org/acscatalysis

EXAFS and FT-IR Characterization of Mn and Li Promoted Titania-Supported Rh Catalysts for CO Hydrogenation

Viviane Schwartz,*[,†] Andrew Campos,[‡] Adefemi Egbebi,[‡] James J. Spivey,[‡] and Steven H. Overbury[†]

[†]Center for Nanophase Materials Sciences and Chemical Sciences Division, Oak Ridge National Laboratory, Oak Ridge, Tennessee 37831, United States

[‡]Cain Department of Chemical Engineering, Louisiana State University, Jesse Coates Hall, S. Stadium Drive, Baton Rouge, Louisiana 70803, United States

ABSTRACT: The effect of Li and Mn promoters on the structure and selectivity of supported Rh catalysts for CO hydrogenation reaction was examined. Infrared spectroscopy and X-ray absorption were used to investigate the adsorption of reactants and local structure of Rh. These techniques were used in combination with reactivity, H_2 chemisorption, and temperature programmed studies to correlate structural characteristics with activity and selectivity during CO hydrogenation of unpromoted Rh/TiO_2 and three promoted Rh catalysts: $Rh-Li/TiO_2$, $Rh-Mn/TiO_2$, and $Rh-Li-Mn/TiO_2$. The presence of a promoter slightly decreases the Rh clusters size; however, no evidence for an electronic effect induced by the presence of Li and Mn was found. Higher turnover frequencies were found for the promoted catalysts, which also showed the lower dispersion. The Li promoter introduces a weakened CO adsorption site that appears to enhance the selectivity to C_{2+} oxygenates. The selectivity to C_{2+} oxygenates varies inversely with the reducibility of Rh metal, that is, the lower the Rh reducibility, the higher the selectivity.

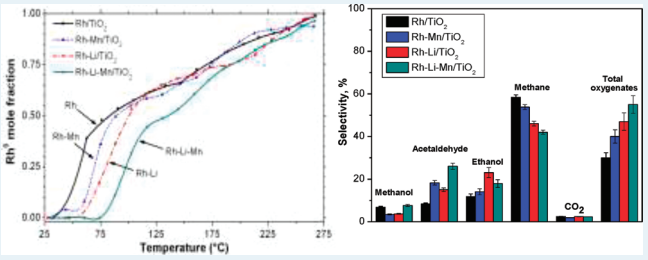

KEYWORDS: ethanol, Rh, promoter, EXAFS, FTIR, CO hydrogenation

1. INTRODUCTION

The interest in Rh and promoted Rh catalysts has been strongly associated with the CO hydrogenation reaction.[1−6] This reaction over rhodium catalysts yields a variety of products, such as methane, methanol, ethanol, and other oxygenates, and hydrocarbons. The product distribution is strongly dependent on the reaction conditions and the presence of promoters. The use of alkali promoters has been shown to be crucial for shifting selectivities toward the thermodynamically less favored products, such as ethanol and C_2^+ oxygenates.[7−9] The role of the alkali promoters is to enhance oxygenate formation by suppressing the hydrogenation activity of Rh, which can lead to C_1 products (methane and methanol).[9,10] This suppression has to be balanced with C−C bond formation so that selectivity to C_1 products is minimized, but sufficient hydrogenation activity is present to form C_2+ oxygenates.[11]

The exact mechanism of oxygenate promotion by alkali addition is still largely unknown. For instance, Luo et al. have claimed that Mn and Li promoters can increase hydrogen spillover, which can take part in the activation of adsorbed CO.[12] Li is believed to increase the electron density of surface Rh, therefore weakening the C−O bond of the adsorbed species.[13] This kind of electronic effect has been investigated using theoretical calculations which point to a correlation between activity (or selectivity) and the electronegativity differences between Rh and the promoter.[14] Another hypothesis is that the promoter may block Rh surface sites, thereby inhibiting reaction steps like CO dissociation that require large ensembles of atoms.[15]

The support can also act as a promoter and alter the selectivity of the CO hydrogenation reaction. Results have been published on titania-supported Rh,[9,16,17] Rh/SiO_2,[1,18−20] and Rh/Al_2O_3 catalysts.[21,22] The presence of surface hydroxyls on supports, such as TiO_2, can have a 2-fold effect: (1) providing anchors for catalyst precursors, which affects the particle size and metal−support interaction;[23−25] (2) altering the catalytic mechanism via coordination of chemisorbed CO at the oxygen end, weakening the C−O bond and facilitating its dissociation.[21,26,27] Here, we use TiO_2 as a support since Rh/TiO_2 has also been found to be more active for CO decomposition and hydrogenation than Rh/SiO_2 or Rh/Al_2O_3.[28]

Our work aims to elucidate the Rh structure and chemical environment when Li and Mn promoters are present on a Rh/TiO_2 catalyst with the ultimate goal of examining the effect of promoters in shifting the selectivity to C_{2+} oxygenates. Infrared spectroscopy has been used as a surface sensitive tool to study the interaction between CO and Rh, which can reveal subtle changes in the character of the TiO_2-supported rhodium. X-ray absorption spectroscopy (XAS) under in situ conditions is used to

Received: June 3, 2011
Revised: August 15, 2011
Published: August 22, 2011

clarify the structure and chemical environment of highly dispersed Rh catalysts, as well as to follow changes of the oxidation state and structure under variable conditions. In this work, we have applied both methods in combination with conventional reaction studies, H_2 chemisorption, and temperature programmed studies to correlate the structural characteristics with the changes of activity and selectivity of the unpromoted Rh/TiO_2, Rh−Li/TiO_2, Rh−Mn/TiO_2, and Rh−Li−Mn/TiO_2 during CO hydrogenation.

2. EXPERIMENTAL SECTION

Catalyst Preparation. A wt. basis formulation with targeted composition of 1%Rh/TiO_2 and 1%Rh-0.1%Li/TiO_2 (yielding a Li/Rh atomic ratio of about 1:1), 1%Rh-0.55%Mn/TiO_2 (yielding a Mn/Rh molar ratio of about 1:1), and 1%Rh-0.1% Li-0.55%Mn/TiO_2 catalysts were prepared using conventional incipient wetness impregnation. Aqueous solutions of Rh-$(NO_3)_3$, $LiNO_3$, and $Mn(NO_3)_2$ were used as metal precursors for the corresponding catalysts. The solutions were co-impregnated on a TiO_2 (Degussa Aerolyst 7710 [based on P25], ∼50 m^2/g) support, dried overnight at 110 °C, and calcined under air for 4 h at 500 °C. The bulk elemental composition was measured on a Varian Vista AX CCD Simultaneous ICP-OES (Inductively-Coupled Plasma Optical Emission Spectroscopy). Brunauer−Emmett−Teller (BET) surface area was obtained using N_2 adsorption at −196 °C in a Quantachrome Autosorb-1 surface area analyzer.

Catalyst Activity Test. Reaction tests at differential CO conversions were carried out in a 1/4″ glass-lined stainless steel fixed bed microreactor system (Altamira 200HP) at 260 and 270 °C and total pressure of 20 bar. Prior to reaction tests, 0.25 g of catalyst was loaded into the reactor and reduced in situ for 2 h in 75% H_2/25% He mixture at 350 °C. CO hydrogenation (H_2/CO = 2) reactions were run at GHSVs of 52800 scc(h g_{cat})$^{-1}$. For each run, the syngas feed was diluted with He to reduce heat effects within the bed; this ensures that the conversion is low enough to keep the oxygenated products in vapor state for online GC/MS analysis. The total inlet flow rate was 220 sccm, consisting of 80 sccm H_2, 40 sccm CO, and 100 sccm He. Reactions were run for at least 1.5 h to achieve steady state, and products were collected during the subsequent 4 h in steady state using an online Agilent GC/MS system (Agilent Technologies 6890N/5975B) equipped with two thermal conductivity detectors (TCD). The line from the reactor exit to the sampling valves was heat traced to prevent products from condensing upstream of the GC/MS. The sampling valves were placed in an isothermal oven and maintained at a temperature of 250 °C. Oxygenates and C_2−C_4 hydrocarbon analysis was done, following GC separation, using a mass selective detector (MSD) while H_2, CO, CO_2, and CH_4 were analyzed by TCD.

H_2 Chemisorption. The number of exposed rhodium surface atoms was determined by H_2 chemisorption using a Quantachrome Autosorb-1. Catalyst samples of approximately 0.3 g were first evacuated at 120 °C for 120 min, reduced at 350 °C in a hydrogen flow for 120 min, and then evacuated at 350 °C for another 120 min. After cooling under vacuum to 40 °C, the H_2 adsorption isotherm was recorded. Subsequently, the sample was evacuated and then a second adsorption isotherm was obtained at the same temperature. The amount of chemisorbed H_2 was obtained by extrapolating the difference isotherm, that is, the irreversible chemisorption, to zero pressure. The metal dispersion (Rh_s/Rh_{tot}) was calculated assuming $H/Rh_s = 1$.

Temperature Programmed Reduction (TPR). Before TPR measurement, catalysts samples of 250 mg were first degassed with He flow at 120 °C for 30 min to remove moisture from ambient storage and then cooled down to RT under He flow. The sample was then exposed to 100 sccm of a 10% H_2/Ar gas mixture, as the reactor temperature was ramped at 5 °C/min from RT to 500 °C. TCD signal corresponding to H_2 consumption was then recorded as a function of temperature.

XAS. The XAS data at the Rh K-edge (23220 eV) were collected at beamline X18B at the NSLS (National Synchrotron Light Source), Brookhaven National Laboratory. The storage ring is operated at 2.5 GeV with a current between 200 and 300 mA, and the beamline is equipped with Si (111) crystals as the monochromator. X-ray absorption was measured in fluorescence mode, by using a large area Passivated Implanted Planar Silicon (PIPS) detector perpendicular to the incoming beam. Spectroscopic information on the Rh-oxidation state was obtained by in situ measurements in a Kapton capillary cell (1/16″ OD) used for time-resolved, temperature dependent studies in which the temperature and the flowing gases were controlled and selected for a given pretreatment condition. The protocol involved (1) extended X-ray absorption fine structure (EXAFS) measurements at room temperature (RT); (2) X-ray absorption near edge structure (XANES) spectra every 15 °C increase of temperature during TPR treatment in 5% H_2/He up to 270 °C; (3) EXAFS measurements at 270 °C under 5% H_2/He; (4) EXAFS measurements under a syngas mixture (feed consisted of H_2 and CO at 2.2 and 1.1 kPa respectively with balance He) at 270 °C. The program XDAP, version 3.2, was used to analyze and fit the data.[29] The data reduction procedure consisted briefly of the following steps: pre-edge subtraction, background determination, normalization, and spectra averaging. The edge position is defined to be the first inflection point on the leading absorption peak. This was calibrated to be 23220 eV for the K-edge of a Rh reference foil. The background in the EXAFS region was approximated using a cubic spline routine and optimized according to the criteria described by Cook and Sayers.[30] Then, the spectra were normalized by the edge-step at 50 eV after the absorption edge. The k^3-weighted and k^1-weighted EXAFS functions were Fourier transformed, filtered, and fitted in R-space. Fourier filtering was used to isolate the contributions of specific shells and to eliminate low frequency background and high frequency noise. Fourier filtering is done by choosing a window in the Fourier transform spectrum and calculating the inverse Fourier Transform of the selected R-range. The interatomic distance (R), the first nearest-neighbor coordination number (CN), the difference of the Debye−Waller factor from the reference ($\Delta\sigma^2$), and the correction of the threshold energy ($\Delta E°$) were treated as free parameters during the fitting. The quality of the fit was estimated from the values of k^{fit} variance (V_k). The variance represents the residuals between the observed and calculated spectrum in the fitted range. Low values of variance indicate a good agreement between the data and model. Fitting analysis using both k^1 and k^3-weighted Fourier transforms was applied to obtain a unique set of CN and $\Delta\sigma^2$ parameters. Those parameters are highly correlated, and there are a number of different combinations of CN and $\Delta\sigma^2$ that can lead to similar fits; however the set of combinations depends on the k-weight factor. Therefore, a unique set of parameters might be found by fitting on both k^1 and k^3-weighted Fourier

Table 1. Measured Composition and BET Surface Area of the Catalysts

catalyst	metal	composition (wt %)[a]	BET surface area (m^2/g)
Rh/TiO_2	Rh	0.90	45
$Rh-Mn/TiO_2$	Rh	1.03	45
	Mn	0.48	
$Rh-Li/TiO_2$	Rh	1.16	43
	Li	0.09	
$Rh-Li-Mn/TiO_2$	Rh	1.07	43
	Mn	0.47	
	Li	0.08	

[a] Measured by ICP.

transforms. To analyze the spectra, simulations of reference compounds using FEFF8.122[31] were used to calculate phase shifts and backscattering amplitude. FEFF references were obtained for Rh−Rh by utilizing crystallographic data of Rh metal, and for Rh−O by utilizing crystallographic data of Rh_2O_3. The S_0^2 (amplitude reduction factor) was found to be 0.8 from the Rh reference foil, and was used in the EXAFS fitting of the sample spectra.

FT-IR. The FTIR measurements were made on a Thermo Electron Nexus 670 spectrometer using a MCT detector. A diffuse reflectance infrared Fourier transform spectroscopy (DRIFTS) cell from Pike Technologies (DiffusIR) was used. It features a small (approximately 6 mL) reaction volume and is capable of temperature control from RT to 900 °C at atmospheric pressure. In a typical experiment, about 50 mg of Rh-based catalyst was inserted into the DRIFTS cell and reduced under 4% H_2/He at a temperature of 350 °C prior to each experiment. A manifold of valves was used to switch gases through the DRIFTS cell. The cell was flushed with He at 350 °C, and the gas flow was switched to 2% CO/He only after lowering the temperature to RT. Spectra were taken under 2% CO flow at RT and at 270 °C. Difference spectra were obtained by subtracting the background taken under He. Spectra were typically recorded at 4 cm^{-1} resolution and could be recorded every 5 s.

3. RESULTS AND DISCUSSION

The composition of synthesized Rh-promoted catalysts as measured by ICP-OES are very close to the nominal targets and are shown in Table 1. Total BET surface area does not significantly vary after impregnation (Table 1). X-ray diffraction patterns of the catalysts showed only peaks consistent with the TiO_2 support phases. Inability to detect the Rh phase may be due to its high dispersion or its low loading. In such cases, XAS proves to be an invaluable resource.

3.1. Rh Surface Area by Selective H_2 Chemisorption. The available active Rh surface area for the catalysts was determined by volumetric H_2 chemisorption, and the results are summarized in Table 2. Decreased capacity for H_2 chemisorption for the Rh−Mn and Rh−Li catalysts is observed, leading to a lower calculated dispersion value compared to the unpromoted Rh. Others have reported a decrease of H_2 and CO chemisorption with the addition of promoters, such as Fe,[16] Li,[32] and V.[33] It is possible that the suppression of chemisorption may be due to the blocking of the Rh sites by the promoter. This suppressed

Table 2. H_2 Chemisorption after Reduction of the Rh-Based Catalysts

	H_2 chemisorbed ($\mu mol/g_{cat}$)[a]		
catalyst	total	irrev	dispersion[b]
Rh	56.9	24.9	54%
Rh−Mn	30.5	16.5	34%
Rh−Li	22.2	13.4	25%
Rh−Mn−Li	71.9	32.7	63%

[a] 5% error in the measurements. [b] Based on the irreversible chemisorption and assuming a stoichiometry of $H/Rh_s = 1$.

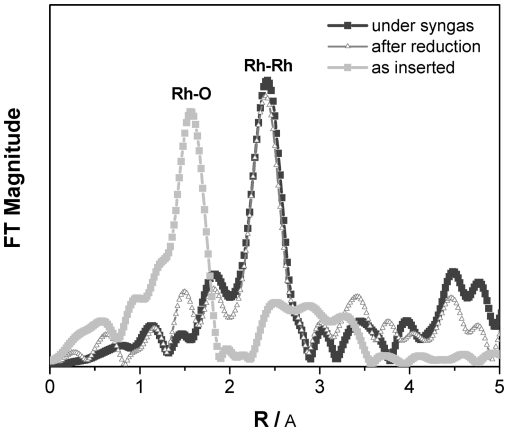

Figure 1. Magnitude of the Rh K-edge k^3-weighted Fourier transform of Rh−Li−Mn/TiO_2 after calcination; after TPR treatment at 270 °C; and, after subsequent exposure to a syngas mixture.

chemisorption does not necessarily hinder the CO hydrogenation activity on the promoted catalysts, since the interfacial sites between the metal and the promoter may be substantially more active than the unpromoted Rh.[33] Interestingly, the addition of both Li and Mn in the doubly promoted catalyst leads to higher H_2 uptake and, therefore, higher dispersion compared to the unpromoted Rh/TiO_2. Higher H_2 uptake for promoted Rh catalysts has also been attributed to H_2 spillover from the metallic Rh to the Mn oxide particles.[14,34] However, both the total and the reversible adsorption curves exhibit a saturation plateau, which could be an indication of absence of such spillover phenomenon.

3.2. Reducibility and Particle Size by EXAFS and TPR. X-ray absorption was used to determine the influence of the promoter(s) over the reducibility and oxidation state of Rh, and to obtain information on the Rh particle size and its atomic surroundings. EXAFS data were recorded for each sample as prepared and after H_2 treatment. Figure 1 shows typical Fourier Transformed EXAFS spectra obtained for one of the samples (Rh−Li−Mn/TiO_2) after calcination, after the TPR treatment, and after exposure to a syngas mixture flow at 270 °C for 30 min. This figure clearly demonstrates Rh_2O_3 is reduced to Rh metallic clusters, as the Rh−O contribution at 2.0 Å disappears and the Rh−Rh contribution at 2.67 Å is formed. No observable peaks were attributed to Rh−Li, Rh−Ti, or Rh−Mn bonds after calcination, after reduction, or under syngas flow; this was true for all promoted catalysts analyzed and indicates no observable mixed metal oxide formation. Additionally, no significant changes were observed for the EXAFS spectra after exposure to the syngas mixture. A comparison of the

dx.doi.org/10.1021/cs200281g |ACS Catal. 2011, 1, 1298–1306

magnitude of the EXAFS function for all the samples after reduction is presented in Figure 2, and the fitting analysis results for all the samples before reduction, after reduction, and under syngas atmosphere are given in Table 3. Note that the distances observed in the Fourier transformed spectra (Figures 1 and 2) are always shorter than the real absorber-backscatterer distances (Table 3) because of the phase shifts. For a bulk Rh metal of fcc crystal structure, the coordination of the first Rh shell located at 2.69 Å would be 12. The CNs obtained for the Rh−Rh shells for the unpromoted and promoted Rh catalysts after reduction were all smaller than the bulk value indicating the presence of small Rh particles. Additionally, the coordination distance shows a contraction in comparison with the bulk value (r = 2.69 Å), which in combination with the low CN, is a strong indication of highly dispersed Rh on the catalyst. The presence of a promoter causes a slight decrease of particle size as indicated by smaller CNs. The size of the Rh particles can be estimated by Rh cluster models with varying numbers of atoms and calculating the average CN.[35,36] Average sizes based on the fitted CN and assuming a spherical model for the Rh−Rh shell are between 1 and 1.5 nm for the unpromoted reduced catalyst and less than 1 nm for the promoted catalysts.[32,37] Under the presence of CO and H_2 at 270 °C, there are negligible changes in the CN and a general shift to slightly higher bond distances for the Rh−Rh clusters. Similar expansion of Rh−Rh bonding upon CO adsorption onto highly dispersed Rh supported particles has been reported in the literature.[37−40]

A detailed picture of the reduction process was developed by following the XANES spectra during the in situ TPR. Figure 3 shows a set of XANES spectra obtained during H_2 reduction of Rh/TiO_2. The intensity of the white line in the Rh K-edge XANES spectrum (Figure 3), which is the first absorption peak centered about 23240 eV, originates from the transition of electrons from the 1s states to the unoccupied p states.[41] Therefore, any variations of the density of unoccupied states because of changes in oxidation state will be reflected in the intensity of the white line. The initially prepared Rh/TiO_2 sample clearly indicates cationic Rh; the transformation of cationic Rh to reduced Rh is easily followed by the decrease of the white line intensity during the H_2 treatment. Another indication of Rh reduction is the shift of the absorption edge to lower energies. Although the final XANES spectrum (after reduction at

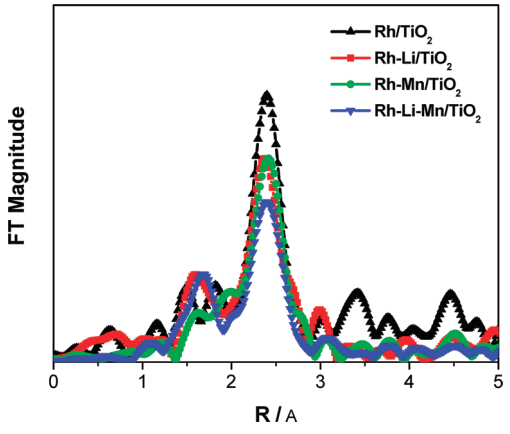

Figure 2. Comparison of the magnitude of the Rh K-edge k^3-weighted Fourier transform of all the Rh supported samples with and without promoters after reduction.

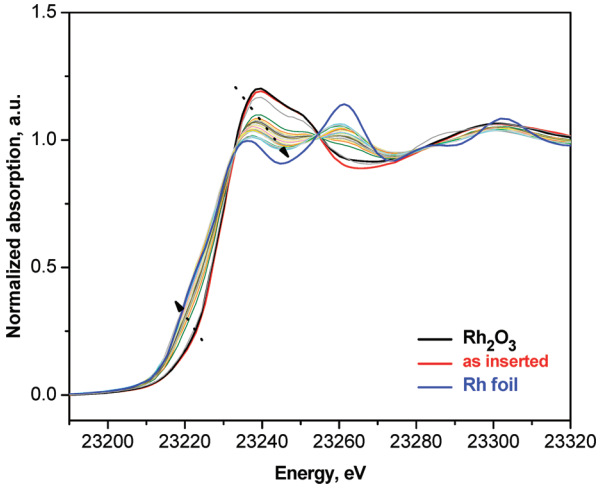

Figure 3. XANES spectra at the Rh K-edge of the Rh/TiO_2 sample during TPR with 5% H_2/He up to 270 °C and soaking at this temperature for another 50 min. Arrows indicate temperature increase. The XANES spectra of the Rh foil and Rh_2O_3 were also measured and used as references.

Table 3. Results of the Curve Fitting of the Rh K-Edge for the Samples after Calcination and after TPR[a]

catalyst		shell	CN	R/Å	$\Delta\sigma^2$ /10^{-3} Å^2	$\Delta E°$ /eV
Rh/TiO_2	as-inserted	Rh−O	5.6 ± 0.6	2.00 ± 0.01	1.4 ± 2.0	4.1
	reduced	Rh−Rh	7.5 ± 0.7	2.67 ± 0.01	5.7 ± 1.6	0.8
	in syngas	Rh−Rh	7.2 ± 0.7	2.68 ± 0.01	4.8 ± 1.6	0.3
$Rh-Li/TiO_2$	as-inserted	Rh−O	5.8 ± 0.5	2.00 ± 0.01	1.3 ± 1.8	5.4
	reduced	Rh−Rh	6.6 ± 0.8	2.64 ± 0.01	6.3 ± 1.9	0.1
	in syngas	Rh−Rh	6.3 ± 0.7	2.66 ± 0.01	5.4 ± 1.8	1.0
$Rh-Mn/TiO_2$	as inserted	Rh−O	5.6 ± 0.5	2.01 ± 0.01	1.1 ± 1.8	3.4
	reduced	Rh−Rh	6.4 ± 0.8	2.64 ± 0.01	6.1 ± 2.0	−1.7
	in syngas	Rh−Rh	5.7 ± 0.7	2.67 ± 0.02	5.9 ± 2.1	0.1
$Rh-Li-Mn/TiO_2$	as-inserted	Rh−O	5.6 ± 0.5	2.00 ± 0.01	0.9 ± 1.7	5.1
	reduced	Rh−Rh	5.9 ± 0.8	2.65 ± 0.02	6.8 ± 2.4	0.3
	in syngas	Rh−Rh	5.7 ± 0.8	2.66 ± 0.02	7.7 ± 2.8	1.1

[a] Fitting results obtained from fluorescence data. For the Rh−O shell, the results show the fitting analysis done using R-space and k^1-weighted function; ΔR from 0.5 to 2.2 Å; Δk from 3.8 to 15 Å^{-1}. For the Rh−Rh shell, the results show the fitting analysis R-space and k^3-weighted function; ΔR from 1 to 3.5 Å; Δk from 3.4 to 14.4 Å^{-1}.

dx.doi.org/10.1021/cs200281g |ACS Catal. 2011, 1, 1298−1306

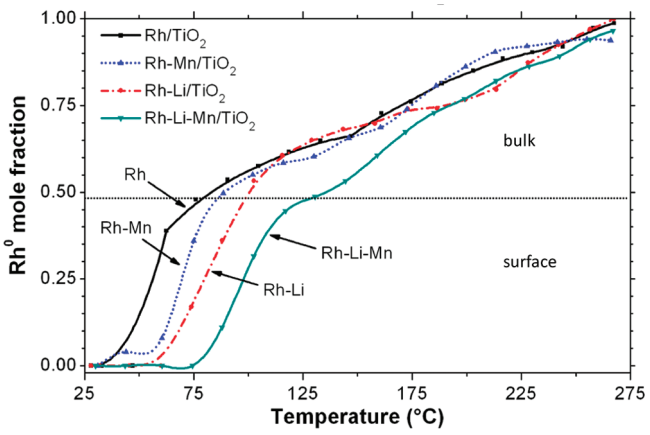

Figure 4. Rh^0 mol fraction as a function of temperature for Li, Mn, Li−Mn promoted Rh, and unpromoted Rh. The horizontal dotted line represents the average mole fraction at which reduction moves beyond surface and into the bulk.

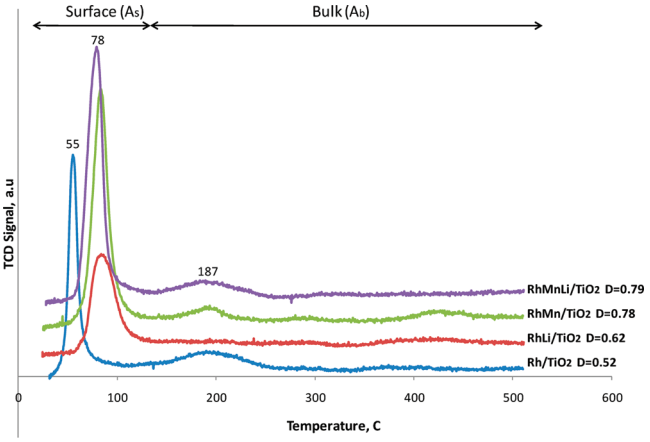

Figure 5. TPR profiles of the Rh supported catalysts after calcination. TPR conditions: 5 °C/min heating rate; RT to 500 °C; 10% H_2/Ar, 50 sccm; sample weight, 0.25 g-cat. Dispersion (D) was calculated by dividing the areas $A_s/(A_s + A_b)$.

270 °C for 50 min) and the XANES observed by Rh foil are not identical, the differences can be attributed to several factors other than differences in the oxidation state, such as the size of the particles and interactions with the support. Rh^0 and Rh_2O_3 XANES reference spectra (also shown in Figure 3) were used to perform a least-squares fitting analysis to determine the Rh^0 content as a function of reduction temperature for all the catalysts measured. Figure 4 shows the variation of Rh^0 content with temperature for the unpromoted and the Li- and Mn promoted Rh/TiO_2. It is clear that the introduction of a promoter shifts the reduction of Rh to higher temperatures, which could be the result of an intimate contact between Rh and the promoters on the surface. A similar increase in the reduction temperature for promoted Rh has also been observed by others.[8,22]

The reduction behavior observed by XANES and the particle size estimated by EXAFS are consistent with the TPR profiles shown in Figure 5. From the literature,[5,42] the low-temperature peak at the TPR curve can be attributed to the reduction of surface Rh oxide species and the smaller high-temperature peak to the reduction of bulk Rh species. Values of dispersion (D) can be estimated from the TPR by dividing the area under the low-T peak (ranging from RT to about 125 °C) by the total area under the low-T and high-T broad features (>125 °C) shown in Figure 5. The values of dispersion obtained by the TPR measurements would indicate particle sizes between 1 and 2 nm assuming a spherical particle model.[43] This is not very different than the sizes estimated by EXAFS, especially taking into account experimental errors and the approximations of assuming a spherical particle model. Rh dispersions estimated from the three different methods described above are summarized in Table 4. Difference among these three independent methods is to be expected, since each of these methods measures different properties of the catalysts. Notably, the dispersions estimated from H_2 chemisorption are generally the lowest while those obtained using EXAFS tend to be the highest (Table 4). EXAFS measures mean Rh CNs, and dispersions were calculated based on the surface-to-volume atomic ratio for a spherical particle model.[36] These values are therefore related to particle size, and the increase in dispersion in all promoted catalysts compared to unpromoted Rh catalysts would be indicative of

Table 4. Comparison of the Rh Metal Dispersion Calculated from Three Different Experimental Methods

	dispersion, %		
catalyst	based on EXAFS	based on TPR	based on H_2 uptake
Rh	68%	52%	54%
Rh−Mn	81%	78%	34%
Rh−Li	80%	62%	25%
Rh−Mn−Li	100%	79%	63%

smaller Rh particle size in the promoted catalysts, especially the doubly promoted catalyst. Hydrogen chemisorption measures the amount of Rh surface atoms that are active for H_2 adsorption and is affected by presence of surface species that block H_2 chemisorption or lower its adsorption energy. Low dispersion values obtained by this method for the promoted and doubly promoted catalysts could be partly attributed to such blocking, even though the Rh particle sizes may actually be smaller. Although EXAFS measurements did not indicate any observable peaks attributed to significant Rh−Li, Rh−Mn or Rh−Ti bonding, it would be difficult to observe a partial covering of the Rh by a promoter phase or a reduced TiO_2 phase. Reduction of the catalysts at 350 °C is well-known to suppress chemisorption (SMSI effect) because of formation of TiO_x overlayers on the active metal.[44] TPR measures the total amount of hydrogen consumption, and dispersion is then calculated by the areal fraction of low-T peak, corresponding to the more readily reduced surface species, by the total area, corresponding to total amount of Rh. Difficulties in interpreting this value arise from imprecise assignment of the peaks since reduction of promoter phases and titania may contribute to the TPR signal. Also the TPR is recorded from samples last calcined at 500 °C while the EXAFS and H_2 chemisorption results are recorded on the catalysts freshly reduced at 270 and 350 °C, respectively.

3.3. Studies of CO Adsorption by FTIR. Infrared spectroscopy was used to probe the interaction of CO and Rh since variations of the carbon−oxygen stretching frequencies of CO chemisorbed on Rh are due to subtle changes in the character and chemical environment of the supported rhodium. Infrared spectra of CO

dx.doi.org/10.1021/cs200281g |ACS Catal. 2011, 1, 1298–1306

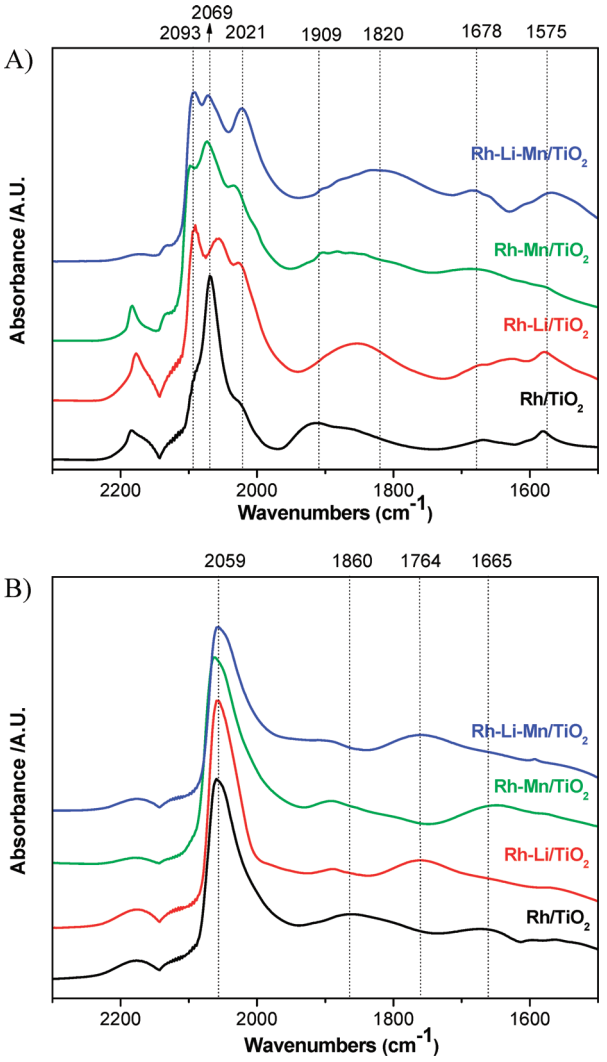

Figure 6. Comparison of the FTIR spectra for CO adsorption at (a) RT and (b) 270 °C over pre-reduced promoted and unpromoted Rh supported catalyst.

adsorption were taken for all catalysts at RT (Figure 6a) and at 270 °C (Figure 6b) after prior in situ reduction in 4% H_2/He at 350 °C.

Interestingly, at RT, there is clear evidence of cationic $Rh^{\delta+}$ even after reduction at 350 °C. This is revealed by the features at 2093 and 2021 cm^{-1} that are attributed to the symmetric and asymmetric carbonyl stretching frequencies of gem-dicarbonyl, $Rh^1(CO)_2$. These features are visible as shoulders in the case of unpromoted Rh/TiO_2 whereas they are clearly discernible for the promoted Rh catalysts. However, both the XANES and EXAFS results for all the catalysts after reduction at 270 °C did not indicate presence of cationic $Rh^{\delta+}$. Either XAS is not sensitive enough to detect small amounts of cationic Rh still present at the surface after reduction or, most likely, the surface suffered some form of chemisorption induced structural modification after exposure to CO. Indeed, Basu et al.[45] have proposed a mechanism that may occur when Rh^0 crystallites are exposed to CO(g) on hydroxylated supports involving the weakening of Rh−Rh bonds by the adsorption of CO on Rh^0 surface sites and the migration of a mobile $[Rh^0\text{-}CO]^*$ species across the oxide surface to isolated OH groups. This effect is also reported by others[37] who have observed a clear change of the EXAFS spectra of supported Rh catalysts after CO adsorption at RT.

As shown in Figure 6b, the gem-dicarbonyl species disappear after raising the temperature to 270 °C under CO flow. At this temperature, the most prominent feature is the vibrational frequency at 2059 cm^{-1} which is attributed to linearly bonded CO adsorbed on reduced Rh metal. The negligible variance of the linear CO frequency indicates that the promoter is not altering the electronic structure of Rh, contrary to what has been previously reported in the literature.[13,46] In addition to the linearly bonded CO on Rh^0, the broad band between 1910 and 1860 cm^{-1} indicates the presence of bridge bonded CO on Rh^0 at reaction temperatures (270 °C). The characteristic broad feature of this band has been ascribed to CO adsorption on different Rh crystalline faces, such as Rh(100) and Rh(111).[47] The most striking difference for the Li-containing catalysts (Rh−Li and Rh−Li−Mn) is the feature around 1760 cm^{-1}, which is too low to be attributable to CO bridge-bonded to several Rh atoms via carbon atom alone. It is attributed to a substantial weakening of the C═O bond or lowering of the bond order. Bridging sites at 1725 cm^{-1} and 1696 cm^{-1} at the metal/oxide interface have been observed previously and were assigned to an adsorption state in which the C atom in each CO molecule is bonded to the metal and the O atom is bonded to a Ti^{3+} cation.[27] In the case of promoted catalysts, this lower wavenumber bridging site has been assigned to a tilted Rh−C—O—M where M is a promoter instead of Ti^{3+}.[26,48] Evidence for such a mixed carbonyl with tilted CO has been hypothesized previously.[49] In either case, such a structure should weaken the C−O bond, leading to surface C produced by enhanced CO dissociation. Both molecularly adsorbed CO and surface carbon species are needed to form higher oxygenates through a balance between C hydrogenation and CO insertion.[7] Here, this band at around 1760 cm^{-1} is only present whenever Li is added as a promoter. Spectra of Rh/TiO_2 and $Rh-Mn/TiO_2$ are very similar and show no evidence of sites around 1760 cm^{-1}.

3.4. Reactivity. Table 5 shows the total CO conversion for the hydrogenation reaction at 260 and 270 °C. As expected, total CO conversion increases with temperature on all catalysts. The conversion values were used to calculate the specific rate of reaction taking the total weight of catalyst as normalization factor since the Rh loading was virtually identical for all the catalysts. However, part of the activity differences observed for the Rh-catalysts could also be attributed to differences in exposed Rh surface area. To account for this factor, the activity must be expressed on the basis of catalytically active Rh rather than total Rh or total weight, that is, as a turnover frequency (TOF). The results from H_2 chemisorption, EXAFS, and TPR experiments can provide different ways for accounting for the fraction of total active Rh on the surface, and Table 5 shows a comparison of TOF values based on the dispersion estimated by the three different methods.

The normalization of rate by exposed Rh did not yield identical TOF values for the four different catalysts, regardless of the method used to calculate the dispersion. This is more evident when using the H_2 uptake as a measure of exposed Rh. In this case, a variation of up to 7-fold in the TOF suggests that indeed there is a promoter effect and that the Rh-based catalyst activity is dependent upon the nature of the promoter. Although the presence of a promoter tends to decrease the amount of exposed Rh, both Rh−Li and Rh−Mn show a higher turnover frequency for CO conversion. This is in agreement with other

dx.doi.org/10.1021/cs200281g |ACS Catal. 2011, 1, 1298–1306

Table 5. CO Conversion and Catalytic Reaction Rates for Two Temperatures[a]

	conversion %[b]		specific rate μmoles CO/g_{cat}/s		TOF (D from H_2 uptake) (s^{-1})		TOF (D from EXAFS) (s^{-1})		TOF (D from TPR) (s^{-1})	
catalyst	260 °C	270 °C	260 °C	270 °C	260 °C	270 °C	260 °C	270 °C	260 °C	270 °C
Rh	0.79 (0.11)	1.03 (0.06)	0.87	1.09	1.89×10^{-2}	2.36×10^{-2}	1.47×10^{-2}	1.83×10^{-2}	1.92×10^{-2}	2.40×10^{-2}
Rh−Mn	1.4 (0.1)	2.06 (0.14)	1.53	2.29	4.48×10^{-2}	6.72×10^{-2}	1.88×10^{-2}	2.82×10^{-2}	1.95×10^{-2}	2.93×10^{-2}
Rh−Li	1.98 (0.24)	2.5 (0.20)	2.18	2.73	7.74×10^{-2}	9.68×10^{-2}	2.42×10^{-2}	3.03×10^{-2}	3.12×10^{-2}	3.90×10^{-2}
Rh−Li−Mn	0.56 (0.07)	0.70 (0.08)	0.65	0.76	1.00×10^{-2}	1.17×10^{-2}	6.29×10^{-3}	7.33×10^{-3}	7.96×10^{-3}	9.28×10^{-3}

[a] Reaction conditions: 20 bar, 52,800scc/h-gcat, H_2/CO = 2/1. [b] Standard errors for a 95% C.I.

Table 6. Comparison of CO Specific Rate and TOF of Rh-Based Catalysts with Values from Literature

		conditions						
catalyst	Rh wt %	P (bar)	T (°C)	H_2/CO	SV (h^{-1})	specific rate μmoles CO/g_{cat}/s	TOF (s^{-1})	ref.
Rh/SiO_2	2	1	220	1.7	86	NR	2.19×10^{-4}	52
$Rh-La_2O_3/SiO_2$	2	1	220	1.7	400	NR	6.78×10^{-4}	52
Rh/TiO_2	2	20	270	1	8000[b]	NR	1.20×10^{-2}	17
Rh/TiO_2	1	20	270	1	8000[b]	NR	2.20×10^{-2}	16
Rh/TiO_2	3	10	300	0.5	1100−11,000	4.8	NR	9
$Rh-Li/TiO_2$	3	10	300	0.5	1100−11,000	1.8	NR	9
Rh−Mn−Li-Zr/SiO_2	1	15	280	2	10,000	NR	1.61×10^{-2}	34
Rh/SiO_2	1.5	20	270	2	18,000[b]	0.12	not available	53
Rh−La−V/SiO_2	1.5	20	270	2	18,000[b]	0.69	not available	53
Rh/TiO_2	1	20	270	2	52,800[b]	1.09	2.36×10^{-2} [a]	this work
$Rh-Li/TiO_2$	1	20	270	2	52,800[b]	2.73	9.68×10^{-2} [a]	this work

[a] Based on dispersion calculated from irreversible H_2 chemisorption. [b] SV in scc/h g_{cat}; NR = not reported.

authors who have also observed a decrease of H_2 chemisorption with higher loadings of promoter accompanied by an increase of turnover frequency.[16] Lower dispersion because of higher reduction temperatures leading to SMSI effect have also shown little effect on the turnover frequency.[16,50] Indeed, others have noted that the SMSI state is abolished in the presence of traces of water, oxygen, or by higher pressures of CO.[51] In contrast to the singly promoted catalysts, the Rh−Mn−Li catalyst presented similar or lower activity (TOF) compared to the Rh catalyst, no matter which method is used to calculate surface active Rh. A comparison with values from literature (Table 6) shows that the specific rates and TOF of the Rh catalysts are in good agreement with several previous measurements.[16,17,34,52,53]

Chuang et al.[11] have described the steps affected by the promoters during CO hydrogenation on Rh-based catalysts, including adsorption and dissociation of carbon monoxide, subsequent hydrogenation, the C−C chain-growth, and the carbon monoxide insertion into a growing chain to form oxygenates. For instance, Mn promoter was found to alter the rate determining step of the CO hydrogenation reaction by promoting both CO insertion and hydrogenation of the adsorbed acyl intermediates.[48] Generally speaking, changes in selectivity are the result of the effect of the promoter on individual reaction steps. Figures 7a and 7b show the product distribution for each catalyst. The major products formed are methane, acetaldehyde, ethanol, and methanol. Increasing the reaction temperature from 260 to 270 °C reduces the total oxygenates and ethanol selectivity while increasing methane formation and total conversion (as seen in Table 5).

Selectivity among catalysts should be compared at the same conversion level, and the very low conversion used in this study allows a good comparison. The Li-promoted catalyst shows the highest activity and highest ethanol selectivity of the four catalysts. The higher ethanol selectivity observed at higher conversions is remarkable since higher conversions usually favors methane formation over C_2^+ oxygenates. The Rh−Mn−Li/TiO_2 catalyst had the highest selectivity to total oxygenates, although this catalyst had the lowest TOF of all the Rh-containing catalyst. Noticeably, Rh−Mn−Li was also the catalyst showing higher selectivity to acetaldehyde, an intermediate for ethanol, possibly because of lower conversion levels achieved. Rh−Mn/TiO_2 shows higher conversions and TOF than the unpromoted Rh catalyst and moderate ethanol selectivity. In general, the presence of a promoter seems to consistently increase the selectivity to oxygenates when compared to the unpromoted Rh catalyst, although the balance between activity and selectivity is dependent on the type of promoter.

It has been hypothesized that electronegativity differences between Rh and the promoter are responsible for changes in activity and selectivity.[14] However, our evidence does not support this hypothesis since FTIR measurements reveal no shifts for the linearly adsorbed CO, which would be evidence of such an electronic effect. Additionally, EXAFS measurements did not reveal any alloy formation, although a partial coverage of Rh by the promoter would not be observable by EXAFS. We propose that the observed changes in selectivity are due to interfacial sites between the Rh and the promoter phase. These sites are selective for oxygenate formation, and their presence is manifest in two

dx.doi.org/10.1021/cs200281g |ACS Catal. 2011, 1, 1298–1306

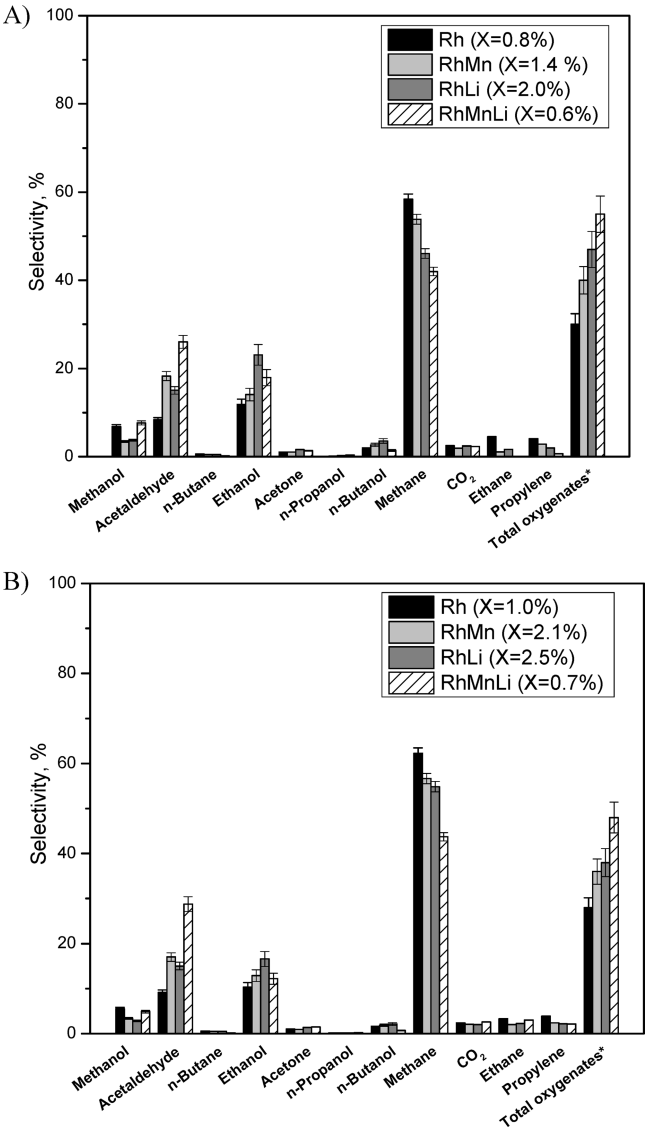

Figure 7. Products selectivity (mol %) for CO hydrogenation over promoted and unpromoted Rh/TiO_2 catalysts at (a) 260 °C, and (b) 270 °C. The CO conversion (X) is provided for each catalyst. Selectivity error bars are based on standard errors for a 95% confidence interval. The total oxygenates does not include CO_2.

observable effects. First, they lead to the formation of a tilted CO bridged adsorption site observed in the FTIR for the Li-containing catalysts. Second, they stabilize the oxidized Rh phase against reduction, which is shown by the higher reduction temperatures for the promoted catalysts. This leads in turn to the observed correlation between the higher selectivity for total oxygenate formation with higher reduction temperature (compare Figure 4 and Figure 7). This promoter-induced site may modify the mechanism of the Rh reactivity by suppression of hydrogen activation on the surface which would prevent CO dissociation as observed by others[32,47] or by hindering CO molecules from being adsorbed hence favoring CO insertion. Furthermore, cationic Rh sites were found to be more active for CO insertion, leading to higher C_2 oxygenates selectivity than reduced Rh sites.[54] Although, in our case, there is no evidence of cationic Rh under reaction conditions, the reducibility character of the Rh metal might affect the CO insertion and oxygenate selectivity, rendering the observed trend of higher C_{2+} oxygenates with lower Rh reducibility.

4. CONCLUSIONS

The effect of Li and Mn promoters on titania supported Rh catalysts were studied by FT-IR and EXAFS and related to their activity and selectivity toward CO hydrogenation. The main conclusions follow.

(1) There is no evidence for electronic effect induced by the presence of Li and/or Mn since there is no observable alteration to the linearly CO bond frequency adsorbed on Rh^0 based on the FTIR studies.

(2) EXAFS spectra did not indicate any clear contribution of Rh−Li or Rh−Mn bonds, therefore there is no indication of alloy formation.

(3) Although the particle sizes estimated by EXAFS were smaller in the case of promoted Rh catalysts, the number of exposed Rh surface atoms was not necessarily higher. Indeed, the Rh−Mn and Rh−Li catalysts showed a lower H_2 uptake, which could indicate that some of the promoters could be covering Rh particles while hindering H_2 chemisortpion. SMSI effects could also lead to a lower dispersion value.

(4) TOF values were different for all the catalysts, indicating a promoter effect. Higher conversions were observed for Rh−Li and Rh−Mn although those catalysts had a lower dispersion, leading to higher apparent TOFs and suggesting that the interfacial sites between the promoter and Rh are the most active ones.

(5) The interaction between Rh and the promoters on the surface leads to a decrease in the reducibility of Rh as observed by XANES and TPR. The ability of a promoter to retard the reduction of the Rh metal should be directly linked to the presence of promoted interfacial sites which would allow this intimate interaction. The selectivity to higher oxygenates is observed to vary inversely with the reducibility of Rh metal. Therefore, we believe that the formation of oxygenates is favored by these interfacial sites. Indeed, the selectivity to oxygenates is as follows: Rh−Mn−Li > Rh−Li > Rh−Mn > Rh.

(6) Li produces a weakened CO adsorbed species, present at reaction temperature, that we propose facilitates oxygenates production. This species is not observed either on the unpromoted catalyst or on the $Rh-Mn/TiO_2$ catalyst, which are the catalysts that have the lowest oxygenate selectivities.

(7) No clear changes on the particle size of Rh were observed by EXAFS when the catalysts were exposed to a syngas mixture. However, a general increase of the Rh−Rh bond distance after syngas exposure may indicate some relaxation of the Rh−Rh bond under low pressure (1 atm) reaction conditions.

(8) CO adsorption at RT leads to a chemisorption induced structural modification and the formation of cationic Rh as evidenced by the presence of gem-dicarbonyl species. This species is less evident for the unpromoted, more easily reducible Rh/TiO_2 catalyst.

(9) Under reaction temperatures and a CO atmosphere, there is no evidence of cationic Rh since gem-dicarbonyl species are not observed in any of the promoted or unpromoted supported Rh catalysts.

dx.doi.org/10.1021/cs200281g |*ACS Catal.* 2011, 1, 1298–1306

AUTHOR INFORMATION

Corresponding Author

*Fax: +1 865 576 1753. E-mail: schwartzv@ornl.gov.

Funding Sources

This work was supported by the U.S. Department of Energy/National Engineering Technology Lab. (Contract no: DE-FC26-06NT43024, Project Officer: Dan Driscoll). A portion of this research was conducted at the Center for Nanophase Materials Sciences, which is sponsored at Oak Ridge National Laboratory by the Division of Scientific User Facilities, U.S. Department of Energy. Use of the National Synchrotron Light Source, Brookhaven National Laboratory, was supported by the U.S. Department of Energy, Office of Science, Office of Basic Energy Sciences, under Contract No. DE-AC02-98CH10886.

REFERENCES

(1) Arakawa, H.; Fukushima, T.; Ichikawa, M.; Natsushita, S.; Takeuchi, K.; Matsuzaki, T.; Sugi, Y. *Chem. Lett.* **1985**, 881.
(2) Bhasin, M. M.; Bartley, W. J.; Ellgen, P. C.; Wilson, T. P. *J. Catal.* **1978**, *54*, 120.
(3) Ehwald, H.; Ewald, H.; Gutschick, D.; Hermann, M.; Miessner, H.; Öhlmann, G.; Schierhorn, E. *Appl. Catal.* **1991**, *76*, 153.
(4) Burch, R.; Petch, M. I. *Appl. Catal., A* **1992**, *88*, 39.
(5) Yin, H. M.; Ding, Y. J.; Luo, H. Y.; Zhu, H. J.; He, D. P.; Xiong, J. M.; Lin, L. W. *Appl. Catal., A* **2003**, *243*, 155.
(6) Forzatti, P.; Tronconi, E.; Pasquon, I. *Catal. Rev.—Sci. Eng.* **1991**, *33*, 109.
(7) Spivey, J. J.; Egbebi, A. A. *Chem. Soc. Rev.* **2007**, *36*, 1514.
(8) Kip, B. J.; Hermans, E. G. F.; Prins, R. *Appl. Catal.* **1987**, *35*, 141.
(9) Chuang, S. C.; Goodwin, J. G.; Wender, I. *J. Catal.* **1985**, *95*, 435.
(10) Choi, Y.; Liu, P. *J. Am. Chem. Soc.* **2009**, *131*, 13054.
(11) Chuang, S. S. C.; Stevens, R. W.; Khatri, R. *Top. Catal.* **2005**, *32*, 225.
(12) Luo, H. Y.; Lin, P. Z.; Xie, S. B.; Zhou, H. W.; Xu, C. H.; Huang, S. Y.; Lin, L. W.; Liang, D. B.; Yin, P. L.; Xin, Q. *J. Mol. Catal. A: Chem.* **1997**, *122*, 115.
(13) Kusama, H.; Okabe, K.; Sayama, K.; Arakawa, H. *Catal. Today* **1996**, *28*, 261.
(14) Mei, D. H.; Rousseau, R.; Kathmann, S. M.; Glezakou, V. A.; Engelhard, M. H.; Jiang, W. L.; Wang, C. M.; Gerber, M. A.; White, J. F.; Stevens, D. J. *J. Catal.* **2010**, *271*, 325.
(15) Chuang, S. C.; Goodwin, J. G.; Wender, I. *J. Catal.* **1985**, *92*, 416.
(16) Haider, M. A.; Gogate, M. R.; Davis, R. J. *J. Catal.* **2009**, *261*, 9.
(17) Gogate, M. R.; Davis, R. J. *Catal. Commun.* **2010**, *11*, 901.
(18) Luo, H. Y.; Zhang, W.; Zhou, H. W.; Huang, S. Y.; Lin, P. Z.; Ding, Y. J.; Lin, L. W. *Appl. Catal., A* **2001**, *214*, 161.
(19) Ichikawa, M.; Fukushima, T. *J. Chem. Soc., Chem. Commun.* **1985**, 321.
(20) Yin, H. M.; Ding, Y. J.; Luo, H. Y.; He, D. P.; Chen, W. M.; Ao, Z. Y.; Lin, L. W. *J. Nat. Gas Chem.* **2003**, *12*, 233.
(21) Burch, R.; Hayes, M. J. *J. Catal.* **1997**, *165*, 249.
(22) Ojeda, M.; Granados, M. L.; Rojas, S.; Terreros, P.; Garcia-Garcia, F. J.; Fierro, J. L. G. *Appl. Catal., A* **2004**, *261*, 47.
(23) Cabero, M. P.; Holgado, M. J.; Rives, V. *Mater. Chem. Phys.* **1991**, *27*, 181.
(24) Usman, U.; Takaki, M.; Kubota, T.; Okamoto, Y. *Appl. Catal., A* **2005**, *286*, 148.
(25) Wachs, I. E.; Deo, G.; Vuurman, M. A.; Hu, H. C.; Kim, D. S.; Jehng, J. M. *J. Mol. Catal.* **1993**, *82*, 443.
(26) Lisitsyn, A. S.; Stevenson, S. A.; Knozinger, H. *J. Mol. Catal.* **1990**, *63*, 201.
(27) Chudek, J. A.; Mcquire, M. W.; Mcquire, G. W.; Rochester, C. H. *J. Chem. Soc., Faraday Trans.* **1994**, *90*, 3699.
(28) Ioannides, T.; Verykios, X. *J. Catal.* **1993**, *140*, 353.
(29) Vaarkamp, M.; Linders, J. C.; Koningsberger, D. C. *Phys. B* **1995**, *208*, 159.
(30) Cook, J. W.; Sayers, D. E. *J. Appl. Phys.* **1981**, *52*, 5024.
(31) Ankudinov, A. L.; Rehr, J. J. *Phys. Rev. B* **1997**, *56*, R1712.
(32) Bando, K. K.; Ichikuni, N.; Soga, K.; Kunimori, K.; Arakawa, H.; Asakura, K. *J. Catal.* **2000**, *194*, 91.
(33) Gao, J.; Mo, X. H.; Goodwin, J. G. *J. Catal.* **2009**, *268*, 142.
(34) Wang, Y.; Luo, H. Y.; Liang, D. B.; Bao, X. H. *J. Catal.* **2000**, *196*, 46.
(35) Frenkel, A. I.; Hills, C. W.; Nuzzo, R. G. *J. Phys. Chem. B* **2001**, *105*, 12689.
(36) Overbury, S. H.; Schwartz, V.; Mullins, D. R.; Yan, W. F.; Dai, S. *J. Catal.* **2006**, *241*, 56.
(37) Vantbilk, H. F. J.; Vanzon, J.; Huizinga, T.; Vis, J. C.; Koningsberger, D. C.; Prins, R. *J. Phys. Chem.* **1983**, *87*, 2264.
(38) Solymosi, F.; Pasztor, M. *J. Phys. Chem.* **1985**, *89*, 4789.
(39) Solymosi, F.; Pasztor, M. *J. Phys. Chem.* **1986**, *90*, 5312.
(40) Vantblik, H. F. J.; Vanzon, J.; Huizinga, T.; Vis, J. C.; Koningsberger, D. C.; Prins, R. *J. Am. Chem. Soc.* **1985**, *107*, 3139.
(41) Fernandez-Garcia, M.; Martinez-Arias, A.; Rodriguez-Ramos, I.; Ferreira-Aparicio, P.; Guerrero-Ruiz, A. *Langmuir* **1999**, *15*, 5295.
(42) Wong, C.; McCabe, R. W. *J. Catal.* **1987**, *107*, 535.
(43) Farrauto, R. J.; Bartholomew, C. H. *Fundamentals of Industrial Catalytic Processes*; Blackie Academic and Professional: New York, 1997.
(44) Tauster, S. J.; Fung, S. C.; Garten, R. L. *J. Am. Chem. Soc.* **1978**, *100*, 170.
(45) Basu, P.; Panayotov, D.; Yates, J. T. *J. Am. Chem. Soc.* **1988**, *110*, 2074.
(46) Kusama, H.; Sayama, K.; Okabe, K.; Arakawa, H. *Nippon Kagaku Kaishi* **1995**, 875.
(47) Fisher, I. A.; Bell, A. T. *J. Catal.* **1996**, *162*, 54.
(48) Brundage, M. A.; Balakos, M. W.; Chuang, S. S. C. *J. Catal.* **1998**, *173*, 122.
(49) Trevino, H.; Lei, G. D.; Sachtler, W. M. H. *J. Catal.* **1995**, *154*, 245.
(50) Vantblik, H. F. J.; Vis, J. C.; Huizinga, T.; Prins, R. *Appl. Catal.* **1985**, *19*, 405.
(51) Ponec, V. *Catal. Today* **1992**, *12*, 227.
(52) Du, Y. H.; Chen, D. A.; Tsai, K. R. *Appl. Catal.* **1987**, *35*, 77.
(53) Subramanian, N. D.; Gao, J.; Mo, X. H.; Goodwin, J. G.; Torres, W.; Spivey, J. J. *J. Catal.* **2010**, *272*, 204.
(54) Chuang, S. S. C.; Pien, S. I. *J. Catal.* **1992**, *135*, 618.